Electro-oxidation of renewable glycerol to value added chemicals over phosphorous-doped Pt/MCNTs nanoparticles

IOP Conf. Series: Materials Science and Engineering **702** (2019) 012025 doi:10.1088/1757-899X/702/1/012025

Electro-oxidation of renewable glycerol to value added chemicals over phosphorous-doped Pt/MCNTs nanoparticles

M S Ahmad[1*], C K Cheng[1, 2], H R Ong [3] and H Abdullah[1], M R Khan[1, 2]

[1]Faculty of Chemical and Natural Resources Engineering, Universiti Malaysia Pahang, Lebuhraya Tun Razak, 26300 Gambang, Pahang, Malaysia.
[2]Centre of Excellence for advanced Research in Fluid Flow (CARIFF), Universiti Malaysia Pahang, Lebuhraya Tun Razak, 26300 Gambang, Pahang, Malaysia.
[3]Faculty of Engineering and Technology, DRB-HICOM University of Automotive Malaysia, Malaysia

*E-mail: chemist019@gmail.com

Abstract. In the present work, Pt/MCNTs and P-dopedPt/MCNTs catalysts were synthesized via hydrothermal method and utilized for glycerol oxidation reaction (GOR). The catalysts were physio-chemically characterized by Brunauer-Emmett-Teller (BET), X-ray diffraction, field emission scanning electron microscopy (FESEM) and transmission electron microscopy (TEM) to investigate pore size, pore volume, structure and morphology of the catalysts. A remarkable reduction in BET surface area was found for P-dopedPt/MNCTs which 1.56 time less than the sole MNCTs is confirming the incorporation of phosphorous into the pore channels of Pt/MCNT. The TEM analysis of P-dopedPt/MCNTS demonstrated the uniform distribution of Pt nanoparticles over multiwalled carbon nanotubes with an average particle size of 6.23 nm. The activity and stability of the catalysts were analysed for GOR using cyclic voltammetry (CV) and chronoamperometry (CA). The CV testing showed the higher current density for P-doped Pt/MCNTs (28.33 A/m^2) which is 2 times higher than the Pt/MCNTs (14.20 A/m^2) current density. The synthesized products were analysed by high performance liquid chromatography (HPLC) analysis which demonstrated the selective synthesis of tartronic acid as a major product with maximum yield. It was found that the P-dopedPt/MCNTs have higher selectivity for tartronic acid and glyceric acid as compared to its counterpart.

1. Introduction

Rapid and overwhelming demands for alternative green fuels to cope with upcoming energy crisis leading towards the utilization of low cost, non-toxic and environment friendly raw materials such as glycerol as fuel of choice [1]. Glycerol produced as a by-product during biodiesel production via esterification of fatty acids of oil and fats [2]. Excess of this by-product founds its applications in electricity production and synthesis of valuable organic compounds by promoting C-C bond cleavage and ultimately complete oxidation to CO_2 [3-5]. Historically, glycerol oxidation was extensively carried out over noble metal catalysts such as Pt, Pd, Ru, Ir and Rh, due to their excellent catalytic properties, although the main disadvantage of Pt and Pd is their deactivation at high reaction time [6]. To overcome this problem, the distribution of metals particles over active supports proved to be a promising technique to enhance the overall activity and selectivity of the catalysts. Among them, carbon nanotubes (CNTs) as inert support drawn continuous attention over past few decades. The unique properties such as high

conductivity, enlarged surface area, unique 1 D structure and chemical stability made MCNTs highly suitable for research and industrial applications [7-8].

The physiochemical properties of MCNTs can be tuned either by surface functionalization or by doping with metallic or non-metallic heteroatoms such as nitrogen (N), phosphorous (P), sulphur (S), boron (B) and cobalt (Co) [9-10]. Hu et al. [11] studied the electro-oxidation of glycerol over CeO_2 supported Pt catalysts, resulting the tartronic acid yield of 40%. Carrettin et al. [12] reported the production of dihydroxy acetone selectivity ranging in between 10-80% over charcoal-supported Pt catalysts within pH 2-3, with the incorporation of Bi and Pt with a glycerol conversion of 80%. Similarly, under mild condition, 1 % Au-supported charcoal or 1% Au-supported graphite, resulted synthesis of glyceric acid with selectivity of 100 % [13]. Similar results have been reported by Gomes et al. [14] which synthesized glyceric acid with a selectivity of 55% and 77% with glycerol conversion of 90% for Pt/C and Pd/C, respectively [14]. The chemical doping of graphene and carbon nano tubes with substitutional dopants such as P, B, N and Si atoms can control the size, degree of dispersion and stability of catalyst in order to improve the activity of catalyst [15].

Herein, we report the facile synthesis of Pt/MCNTs and P-dopedPt/MCNTs catalysts via hydrothermal method and utilized for GOR. The physical properties of the catalysts were analysed by using BET, XRD, and TEM. While the electro-chemical studies have been done by conducting cyclic voltammetry (CV) and chronoamperometry (CA) measurements. High performance Liquid chromatography (HPLC) analysis demonstrated the selective synthesis of mesoxalic acid.

2. Experimental

2.1. Chemical reagents and materials

Hexachloroplatinic (IV) acid hexahydrate ($H_2PtCl_6.6H_2O$), was purchased from Merck, Germany. While glycerol anhydrous, phosphorous pentoxide (P_2O_5), hydrazine and Nafion® 117 solution (for ink preparation) were purchased from Sigma-Aldrich, USA. The chemicals are in analytical reagent grade, so used without any further purification.

2.2. Catalyst synthesis

The hydrothermal method was adopted to synthesize the P-doped Pt/MCNTs and Pt/MCNTs catalyst by using hydrazine as reducing agent. In brief, 5 mL of $H_2PtCl_6.6H_2O$ aqueous solution was mixed with 450 mg of phosphorous pentoxide (aqueous solution) for P-dopedPt/MCNTs catalysts. The resulting mixture was put on sonication for 60 min at ambient temperature. The colour of the mixture was light yellow (for both the catalysts) representing that the Pt is in unreduced form. Afterward, hydrazine was added drop wisely to reduce the Pt and was put on sonication for more 30 min. Thereafter, the reduced mixture was then transferred to a hydrothermal reactor and 800 mg of activated MCNTs was added into it. The whole assembly was then kept in an oven at 120 ºC temperature for 5 h. The residue was taken out from cooled vessel and centrifugal washing was carried out thrice with distilled water followed by drying at 100 °C in a vacuum oven. After complete drying, the final sample was grinded using a piston mortar and stored for further physiochemical studies

2.3. Physiochemical Characterization

The X-ray diffraction patterns of P-dopedPt/MCNTs and Pt/MCNTs were taken using a Rigaku Miniflex diffractometer, with the Cu Ka radiation (1.54 Å) X-ray generator at 30 kV and 15 mA The Scherer's equation ($d = 0.9\ \lambda/\beta\ \cos\theta$) was used to determine the crystallite size of the catalyst for 111 peak

The Bruauner, Emmett, Teller (BET) analysis was used to measure the specific surface area, pore size and pore volume of the catalysts. A Micrometrics system (Model ASAp-2000) was used to analyse the sample using a vacuum pressure of 6.67 Pa, and a temperature of 77 K. The degassing of the samples was carried out at 473.15 K for 5 h.

The quantitative measurement of the size distribution, particle size, and morphology of the catalysts was carried out by direct imaging of nanoparticles. A Tecnai G2 20S-TWIN, with accelerating voltage of 220 kV. TEM was employed to examine the structural properties of the electrocatalysts. The sample

for transmission electron microscopy (TEM) was prepared by suspending a 0.1 mg of catalyst powder in an isopropyl alcohol solution followed by sonication for an hour.

2.4. Electrochemical Characterization of Catalyst

A three electrode assembly along with a Pt counter electrode, Ag/AgCl (sat. KCL) as reference electrode and catalyst pasted glassy carbon (GC) as the working electrode were used to conduct the electrochemical studies. A microcomputer-controlled Potentiostat/Galvanostat NOVA 1.10 was used to perform CV and CA analysis. An oxygen free (N_2 bubbled) 0.5 M H_2SO_4 solution was used as electrolyte to perform the CV for electrochemical surface area (ECSA) measurement using equation 1.

$$\mathrm{ECSA} = \frac{Q_{Pt}}{W_{Pt}\ S\ C} \tag{1}$$

where Q_{Pt} is the area calculated by integration of the total charge corresponding to reduction peak of PtO, W_{Pt} is Pt content deposited on glassy electrode (~ 0.157 mg based on the 0.3 µL ink used), S is the charge density for reduced PtO monolayer: 210 µC/cm^2 and C is the scan rate: 0.05 V/s.

While, 0.5 M glycerol and 0.5 M KOH solution was employed as electrolyte for GOR analysis. Prior to each CV test, the electrolyte solution was bubbled with N_2 for 60 min to remove the excess oxygen. The CV curves were obtained at a scan rate of 0.05V/s under inert environment. The catalyst stability against poisoning intermediates was measured by performing CA analysis at -0.28 V for 3600 s in alkaline medium. The samples were also taken during CA analysis for product separation and quantification through HPLC.

2.4.1. Catalyst ink and working electrode preparation

A catalyst ink was prepared for working electrode preparation for each electrochemical study. In a typical procedure, a 0.02 g of fine catalyst powder was weighted in a glass vessel and mixed with 0.15 mL of Nafion® 117 (5% solution and 240 mL of isopropyl alcohol. The mixture was put on stirring overnight in order to completely homogenize. Afterwards, a 0.3 µL of ink was taken using micropipette and transferred onto a cleaned GC electrode (~0.8 cm^2 area), followed by drying at 80 °C in a vacuum oven overnight. The electrode surface was cleaned by cyclizing through CV within a potential window of (-0.2 V -1.4 V @ 0.01 V/s) and (-0.8 V -0.4 V @ 0.05 V/s) for ECSA and GOR analysis, respectively.

2.5. Product distribution analysis by High performance Liquid chromatography (HPLC)

An Agilent 1260, furnished with ultraviolet (210 nm) and refractive index detector (RID). The Phenomenex HPLC column, Model: Rezex ROA® (4.6 mm × 250 mm, 5 mm) was used to perform the chromatographic analysis for GOR products. The column was kept at 65 °C and the wavelength employed was 210 nm (maximum absorbance for organic compounds). The RID detector was kept at 35 °C. The sample injection volume was 10 µL and eluent flow was set at 0.7 mL/min. The mobile phase was 3 mmol H_2SO_4. The possible GOR products were compared with standard samples for identification. The product selectivity was calculated using equation (2).

$$\mathrm{Selectvity} = \frac{n_j}{\Sigma n_j} \times 100\% \tag{2}$$

where n_j is the number of moles of individual product and $\sum n_j$ is the sum of all the products obtained during HPLC analysis. The identification of the products was carried out by comparison with standard samples.

3. Results and discussion

3.1. X-ray diffraction analysis (XRD)

The X-ray diffraction patterns of MCNTs, Pt/MCNTs, and P-dopedPt/MCNTs are shown in the figure 1. The diffraction peaks at 2θ of 43.41° and 53.86° were found for MCNTs. While the diffraction peaks for Pt/MCNTs and P-dopedPt/MCNTs were located at 2θ of 40.00°, 46.24°, 67.85° and 39.886°, 46.22°, 67.83°, respectively corresponding to (111), (200) and (220) lattice planes.

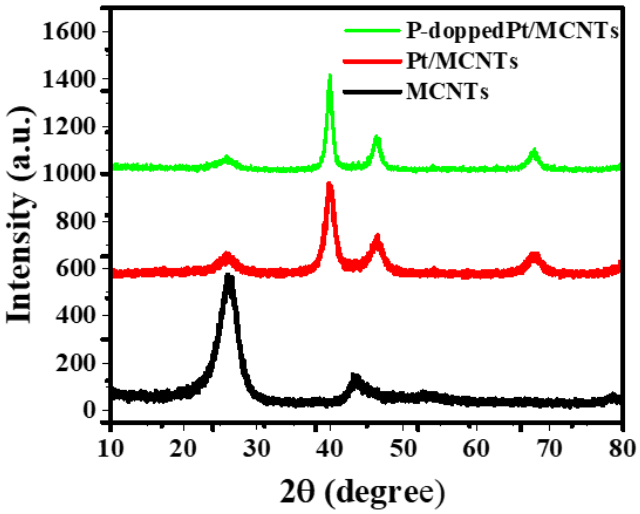

Figure 1. XRD analysis of MCNTs, Pt/MCNTs and P-dopedPt/MCNTs.

Regardless of the catalyst, a strong peak at ca. 2θ ~ 26° was shown for all the catalysts, which corresponds to MCNTs graphitic structure. A typical face centered cubic lattice structure was illustrated from the peak positions for Pt, and Pt alloy catalysts (COD: 1011107). Besides, the XRD pattern were similar for both the catalysts. There was no typical peak detected for phosphorous. In addition, the intensity of these peaks were slightly increased after the addition of phosphorous. Moreover, a negative peak shift (2θ = 0.02) has been observed for P-dopedPt/MCNTs for 220 lattice plane. This revealed that the lattice size of the P-dopedPt/MCNTs catalyst expanded due to incorporation of P into pore channels of Pt/MCNTs. These findings are further confirmed by the calculation of average crystallite size for Pt/MCNTs and P-dopedPt/MCNTs catalysts. The average crystallite sizes of 4.27 nm and 6.24 nm were calculated (for 220 lattice plane) for Pt and P-dopedPt respectively. The increase in average crystallite size for P-dopedPt justified the above statement and also confirmed the incorporation of P and alloy formation with Pt. In one of the recent studies, it was found that the incorporation of Pd into Pt increased the particle size and the crystallite size [16]. A similar explanation has been reported by Ref. [37] for the negative peak shift for incorporation of P into Pt/MCNTs [17]. The d- spacing was also calculated for all the catalysts and values were 0.13801 nm, and 0.13805 nm for Pt/MCNTs and P-dopedPt/MCNTs respectively. The XRD crystallite size for P-dopedPt/MCNTs is line with TEM particle size (6.23 nm).

3.2. BET analysis

The N_2 adsorption and desorption curves for all the materials (MCNTs and electrocatalysts) are presented in figure 2.

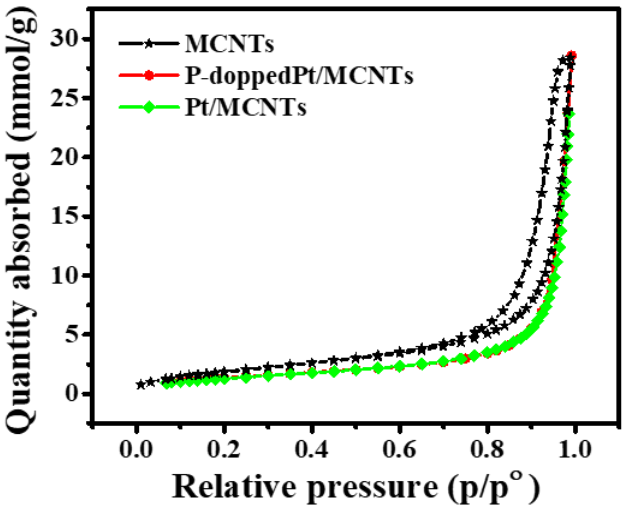

Figure 2. BET analysis of MCNTs, Pt/MCNTs and P-dopedPt/MCNTs.

While all the calculated results for specific surface area and pore size are shown in table 1.

Table 1. Physical properties of MCNTs, Pt/MCNTS and P-dopedPt/MCNTs.

Catalyst	[a] Specific Surface Area (m^2/g)	[a] Pore Volume (cc/g)	[b] Crystallite size (nm)	[c] Crystallite size (nm)
MCNTs	179.30	1.04	-	-
Pt/MCNTs	112.39	0.90	4.27	3.45
P-dopedPt/MCNTs	114.43	1.03	6.24	6.23

[a] Calculated form BET analysis.
[b] Calculated form XRD analysis.
[c] Calculated form TEM analysis.

The Pt/MCNTs, P-dopedPt/CNTs and MCNTs, followed the type-IV adsorption-desorption isotherms characteristics [18]. The MCNTs showed the highest specific surface area as compared to Pt/MCNTs and P-doped/MCNTs which is in an order of 1.59 and 1.56 times respectively. In one of the recent studies by Ref. [19] explained that the reduction in pore size distribution in comparison to MCNTs is dependent to the functional groups along the catalyst surface. While the decrease in total pore volume is through anchoring the functional groups [19]. Likewise, Ref. [20] obtained an increase in a BET surface area for acid (HCL, HF and HNO_3) treated MCNTS and explained this is due to the removal of the inorganic constituents after acid treatment [20]. These results demonstrated that the reduction in surface area of metal catalysts compared to MCNTs can be attributed to the blocking of pores and channels of MCNTs and in agreement with the published literatures [21-23].

3.3. Transmission electron microscope analysis (TEM)

The morphology, particles size and distribution of the metal nanoparticles were revealed by TEM analysis as shown in figure 3.

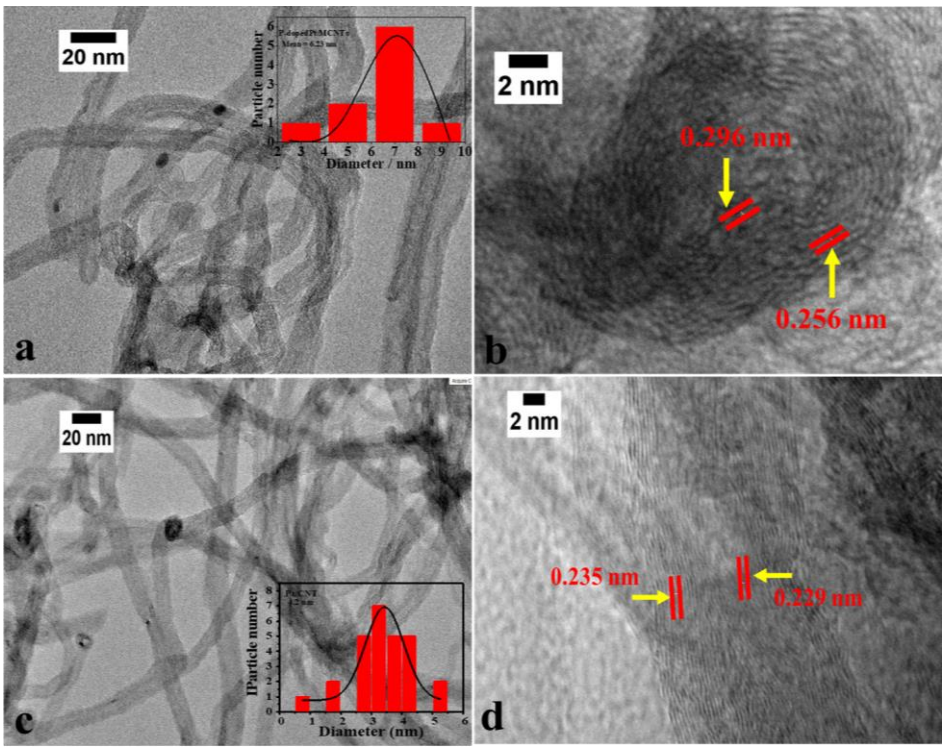

Figure 3. TEM images (a&b); P-dopedPt/MCNTs, and (c&d); Pt/MCNTs, with histograms (insight).

An average particle diameter of 3.45 nm and 6.23 nm was measured using image J software for Pt/MCNTs and P-dopedPt/MCNTs respectively. All the catalysts shown the uniform particle distribution while some of aggregation was also observed for P-doped Pt/MCNTs catalyst which could be attributed to the fast reduction of Pt [24]. The TEM results are in close agreement with XRD data showing almost the similar crystallite size for P-dopedPt/MCNTs (see table 1). In addition, the average atomic spacing (d-spacing = 0.276 nm) was calculated using ImageJ software (figure 3b) for the doped catalyst showing a slight increase which might be due to higher crystallite size (in consistent with XRD).

3.4. Electrochemical characterization

3.4.1. Cyclic Voltammetry (CV)

The electrocatalytic activities of Pt/MCNTs and P-dopedPt/MCNTs were measured in 0.5 M H_2SO_4 and 0.5 M glycerol/0.5 M KOH electrolytes for ECSA and GOR respectively at a scan rate of 0.05 V/s (figures 4(a) and 4(b)).

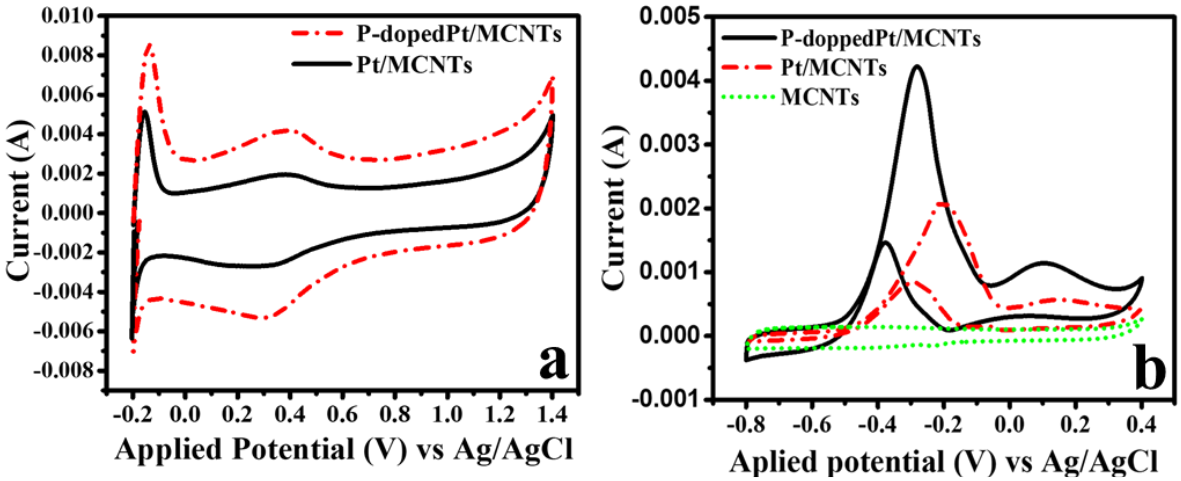

Figure 4. CV curves of Pt/MCNTs and P-dopedPt/MCNTs: (a) ECSA calculation in N_2 saturated 0.5 M H_2SO_4 @ 0.05V/s, (b) glycerol oxidation reaction in 0.5 M glycerol/0.5 M KOH @ 0.05V/s.

As shown in figure 4a, irrespective of the nature of the catalyst, three prominent electrochemical areas are represented in CV profile for both catalysts including double layer capacitance, PtO oxide formation (anodic seep) and PtO oxide reduction (cathodic sweep). Moreover, the formation of surface oxides for P-dopedPt/MCNTs observed at 0.40 V while 0.34 V for Pt/MCNTs, which is 0.06 times, less than the doped catalyst. In contrary, the reduction of these oxides occurs at (0.32 - 0.0 V) and (0.34 - 0.00 V) respectively vs Ag/AgCl for P-doped Pt/MCNTs and Pt/MCNTs.

In addition, the presence of only forward peaks (anodic) in both sweeps demonstrated the irreversibility of the GOR [25-27]. The P-dopedPt/MNCTs showed a higher current density (28.33 A/m^2) as compared to Pt/MCNTs (14.20 A/m^2) which is 1.99 folds higher than the counterpart, indicating the higher GOR activity for P-dopedPt/MCNTs. The ECSA was calculated for both the catalysts and values are presented in table 2.

Table 2. ECSA calculation for Pt/MCNTs and P-dopedPt/MCNTs in 0.5 M KOH @ 50 mV/s.

Catalyst	* I, (A/m^2)	# ECSA, (m^2/g)	Δ I, (A/m^2)
P-dopedPt/MCNTs	28.33	670.95	0.83
Pt/MCNTs	14.20	548.19	0.13

* Current density, measured from CV in 0.5 M glycerol/0.5 M KOH @ 0.05 V/s.
# Electrochemical surface area, measured from CV in 0.5 M H_2SO_4 @ 0.05 V/s.
Δ Current density, measured from CA in 0.5 M glycerol/0.5 M KOH.

While the respective CV curves are shown in figure 4(b). The P-dopedPt/MNCTs demonstrated 1.22 times higher ECSA as compared to Pt/MCNTs catalyst. The higher ECSA for P-dopedPt/MNCTs ascribed to the better dispersion of metal nanoparticles over multi walled carbon nanotubes support [28-29]. It also demonstrated the high availability of effective surface area for the conversion of glycerol to valuable products. Moreover, the incorporation of P into Pt lattice can also enhance the CO poisoning resistance of the catalyst due to higher oxidizability of the catalyst due availability of excess oxygen-containing species [16, 30].

Since the GOR is carried out in an alkaline medium (pH ~ 13) which also facilitates the rate of glycerol oxidation reaction either through deprotonation of the hydroxyl group or desorption of the acid (H^+ ions) from the metal resulting to suppress the rate of CO poisoning [31-33]. Thus a higher current density, lower poisoning rate and high ECSA for P-doped catalyst in comparison to Pt/MCNTs account for the higher activity of the P-doped catalyst for GOR.

3.4.2. Chronoamperometry analysis (CA)

The durability of the as prepared catalysts was measured by performing the CA tests at – 0.28 V for 3600 s (figure 5) and current densities were calculated and presented in Table 2. Regardless of the catalysts, current density abruptly decayed at the initial stage of the reaction while it becomes almost stable at the intermediate stage and finally becomes constant near the completion of reaction. This CA trend revealed that the rate of GOR is higher at the start and intermediate state of reaction indicating the high availability of active sites facilitating the conversion of glycerol to products. While a decrease at final stage clearly demonstrated the poisoning of the reaction sites due to adsorbed oxygenates (CO & CO_2). In addition, it was also found that the current density for P-doped/Pt/MCNTs is 6.38 times higher than the Pt/MCNTs representing the high rate of GOR due to incorporation of P. While a slight reduction at the final stage can be ascribed due to pore blocking of the catalyst [34, 35]. These results are in agreement with the findings reported by Ref. [34] for bimetallic PtPd catalyst for ethanol electro-oxidation [36].

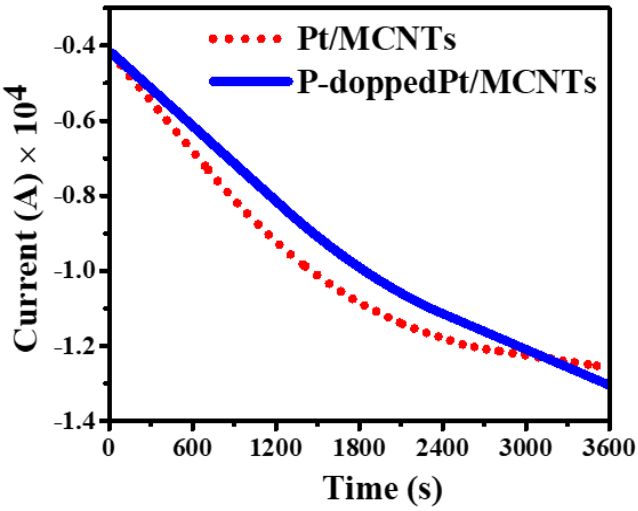

Figure 5. CA curves for Pt/MCNTs and P-dopedPt/MCNTs in 0.5 M glycerol/0.5 M KOH.

3.5. Products Analysis by HPLC

The sample solution from glycerol oxidation reaction is collected during CA test at regular interval of 15 min and products were separated by applying HPLC. Since the glycerol is polyol with complex structure and provides a range of reactive sites over primary and secondary carbons. Thus the complete oxidation of glycerol to organic products (GTO) is susceptible primarily due to slow kinetics and the high energy barrier of C-C bond breaking. In addition, the possibility of complete oxidation is also less due to bulkiness (hydroxyl groups) of the nucleophilic centre providing stearic hindrance to attacking nucleophiles [37]. That reason, partial oxidation of the glycerol produced glyceraldehyde (GALD), tartronic acid (TAT), glyceric acid (GLY) and mesoxalic acid (MOXA) in their salt form but described as acid for simplicity in the paper.

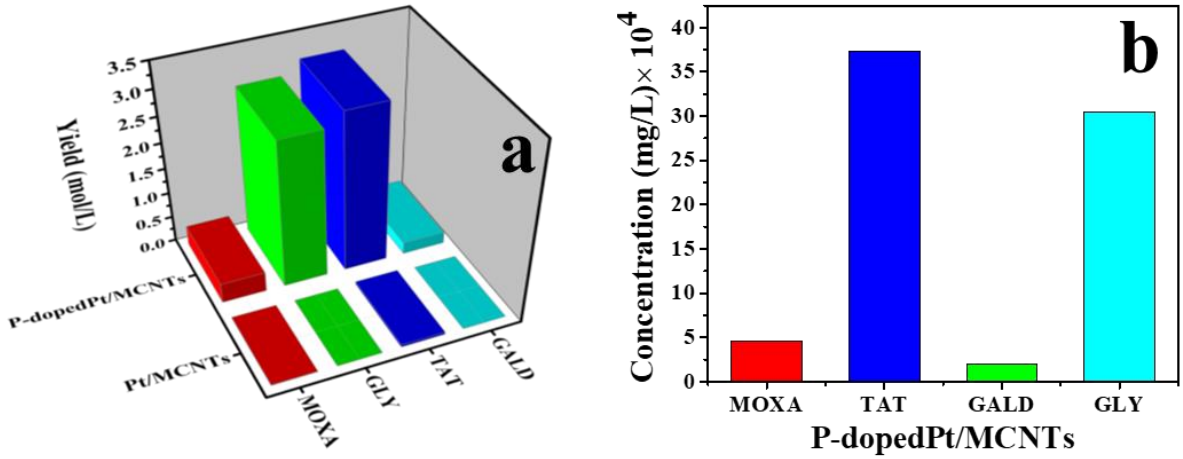

Figure 6. (a) Product distribution for Pt/MCNTs and P-dopedPt/MCNTs in 0.5 M glycerol/0.5 M KOH, (b) product selectivity for P-dopedPt/MCNTs.

Figure 6(a) presented the products distribution for P-dopedPt/MCNTs and Pt/MCNTs. It can be clearly seen that the nature of the products is similar for both the catalysts indicating that the route of reaction is unaltered even after the incorporation of P. while the product yield was enhanced for P-doppedPt/MCNTs. The tartronic acid (TAT) and glyceric acid (GLY) was separated as the major oxidation product while small quantities of mesoxalic acid (MOXA) and glyceraldehyde were also found. In addition, TAT and GLY was found in high yield for P-dopedPt/MCNTs as compared to Pt/MCNTs. This could be explained due to the higher ECSA and stability of the doped catalyst provided due to the incorporation of the P resulting an enhancement in rate GOR.

Furthermore, the selectivities of all the products during GOR of P-doppedPt/MCNTS catalyst were calculated and showed in figure 6b. It is worth mentioning, that TAT have the highest selectivity (~ 47%) which is 1.2 times higher than GLY. While GLY has the second highest selectivity around 40%. The higher yield and better selectivity of the catalyst can ascribe to role of P doping by reducing the accumulation of carbonaceous intermediates and increasing the OH^{-1} availability. The Ref. [24] studied the detailed mechanism for formation and oxidation of carbonaceous intermediates (CO & CO_2) through involvement of hydroxyl ions.

The enhancement in yield of desired C3 compounds acid can be attributed to the strong adsorption of the glycerol molecules with exposed P-dopedPt/MCNTs reactive sites along with uniform distribution of nanoparticles over activated MCNTs support. These results conclude that the incorporation of non-metal P into channels of Pt/MCNTs can remarkably enhance the activity, stability and selectivity of the desired products while keeping the glycerol oxidation pathway unchanged.

4. Conclusions

Highly dispersed P-dopedPt and Pt nanoparticles supported over multiwalled carbon nanotubes (MCNTs) were prepared to study the possible products synthesis from GOR. Through doped P and selectively modified synthetic process of the electrocatalysts, interaction of the non-metal with MCNTs supported noble metal catalyst was researched. The electrochemical analysis suggested the high activity and stability for the P-dopedPt/MCNTs catalyst in comparison to undoped Pt/MCNTs catalyst. In addition, a higher product yield and selectivity of TAT and GLY were also obtained through selective GOR. The enhancement in C3 products yield along with high current density (28.33 A/m^2) ECSA (670.95 m^2/g) and better stability can be attributed to the incorporation of P and strong interaction between metal particles and support. Therefore, P-dopedPt/CNTs can served as an efficient selective catalyst for the valuable products synthesis from electro-oxidation of glycerol at ambient temperature.

Acknowledgements
The authors thank Universiti Malaysia Pahang, Malaysia for providing financial assistance for this project under PGRS-180335.

References

[1] Hunsom M and Saila P 2013 *Int. J. Electrochem. Sci.* **8** 11288-300
[2] Zhou C H C, Beltramini J N, Fan Y-X and Lu G M 2008 *Chem. Soc. Rev.* **37** 527-49
[3] Arechederra R and Minteer S 2009 *Fuel Cells* **9** 63-9
[4] Painter R M, Pearson D M and Waymouth R M 2010 *Angew. Chem. Int. Ed.* **49** 9456-9
[5] Xin L, Zhang Z, Wang Z and Li W 2012 *Chem. Cat. Chem.* **4** 1105-14
[6] Kostecka M, Kowalska D, Kozłowska M and Kowalski B 2013 *J. Oleo Sci.* **62** 893-900
[7] Machado B F, Oubenali M, Axet M R, Nguyen T T, Tunckol M, Girleanu M, Ersen O, Gerber I C and Serp P 2014 *J. Catal.* **309** 185-98
[8] Brandner A, Lehnert K, Bienholz A, Lucas M and Claus P 2009 *Top. Catal.* **52** 278-87
[9] Wepasnick K A, Smith B A, Schrote K E, Wilson H K, Diegelmann S R and Fairbrother D H 2011 *Carbon* **49** 24-36
[10] Su D S, Perathoner S and Centi G 2013 *Chem. Rev.* **113** 5782-816
[11] Hu W, Lowry B and Varma A 2011 *Appl. Catal. B: Environ.* **106** 123-32
[12] Carrettin S, McMorn P, Johnston P, Griffin K, Kiely C J and Hutchings G J 2003 *Phys. Chem. Chem. Phys.* **5** 1329-36
[13] Lakshmanan P, Upare P P, Le N-T, Hwang Y K, Hwang D W, Lee U-H, Kim H R and Chang J-S 2013 *Appl. Catal. A: Gen.* **468** 260-8
[14] Gomes J F, Gasparotto L H and Tremiliosi-Filho G 2013 *Phys. Chem. Chem. Phys.* **15** 10339-49
[15] Tang Y, Yang Z, Dai X, Ma D and Fu Z 2013 *J. Phys. Chem. C* **117** 5258-68
[16] Carvalho L L, Tanaka A A and Colmati F 2017 *J. Solid State Electr.* 1-11
[17] Yang G, Chen Y, Zhou Y, Tang Y and Lu T 2010 *Electrochem. Commun.* **12** 492-5
[18] Tamilarasan P and Ramaprabhu S 2014 *J. Mat. Chem. A* **2** 14054-63
[19] Kohantorabi M, Giannakis S and Gholami M R 2019 *Appl. Catal. A: Gen.*
[20] Wang S and Lu G M 1998 *Carbon* **36** 283-92
[21] Miguel S R, Heinen J C, Castro A A and Scelza O A 1989 *React. Kinet. Catal. L.* **40** 331-5
[22] Torres G C, Jablonski E L, Baronetti G T, Castro A A, de Miguel S R, Scelza O A, Blanco M D, Pen˜a Jiménez M A and Fierro J L G 1997 *Appl. Catal. A: Gen.* **161** 213-26
[23] Hwang S-W, Rather S-u, Naik M-u-d, Soo C S and Nahm K-S 2009 *J. Alloy. Compd.* **480** L20-L4
[24] Zhou W J, Song S Q, Li W Z, Zhou Z H, Sun G Q, Xin Q, Douvartzides S and Tsiakaras P 2005 *J. Power Sources* **140** 50-8
[25] Yang G, Zhou Y, Pan H-B, Zhu C, Fu S, Wai C M, Du D, Zhu J-J and Lin Y 2016 *Ultrason. Sonochem.* **28** 192-8
[26] Hong W, Shang C, Wang J and Wang E 2015 *Energy Environ. Sci.* **8** 2910-5
[27] Li S, Lai J, Luque R and Xu G 2016 *Energy Environ. Sci.* **9** 3097-102
[28] Cha B-C, Jun S, Jeong B, Ezazi M, Kwon G, Kim D and Lee D H 2018 *J. Power Sources* **401** 296-302
[29] Bharti A and Cheruvally G 2018 *Int. J. Hydrogen Energ.* **43** 14729-41
[30] Arroyo-Gómez J J, Barrera D, Castagna R M, Sieben J M, Alvarez A E, Duarte M M E and Sapag K *Chem. Cat. Chem.*
[31] Geraldes A N, Silva D F, Silva J, Souza R F, Spinacé E V, O Neto A, Linardi M and Santos M C 2014 *J. Braz. Chem. Soc.* **25** 831-40
[32] Frota Jr E F, de Barros V V S, de Araújo B R, Purgatto Â G and Linares J J 2017 *Int. J. Hydrogen Energ.* **42** 23095-106
[33] Geraldes A N, da Silva D F, e Silva L G d A, Spinacé E V, Neto A O and dos Santos M C 2015 *J. Power Sources* **293** 823-30

[34] Dutta A and Datta J 2013 *Int. J. Hydrogen Energ.* **38** 7789-800
[35] Dutta A, Mondal A and Datta J 2015 *J. Power Sources* **283** 104-14
[36] Datta J, Dutta A and Biswas M 2012 *Electrochem. Commun.* **20** 56-9
[37] Zhang Z, Xin L and Li W 2012 *Appl. Catal. B: Environ.* **119** 40-8